AGU PUBLICATIONS

JGR

Journal of Geophysical Research: Biogeosciences

RESEARCH ARTICLE
10.1002/2014JG002685

Key Points:
- Permafrost modeling at the West Yamal shelf documents a highly dynamic system
- Continuous subsea permafrost is <250 m thick and limited to water depth <20 m
- Tapering seaward permafrost governs seafloor gas escape in water depths >20 m

Correspondence to:
A. Portnov,
portnovalexey@gmail.com

Citation:
Portnov, A., J. Mienert, and P. Serov (2014), Modeling the evolution of climate-sensitive Arctic subsea permafrost in regions of extensive gas expulsion at the West Yamal shelf, *J. Geophys. Res. Biogeosci.*, *119*, 2082–2094, doi:10.1002/2014JG002685.

Received 4 APR 2014
Accepted 20 SEP 2014
Accepted article online 1 OCT 2014
Published online 17 NOV 2014

Modeling the evolution of climate-sensitive Arctic subsea permafrost in regions of extensive gas expulsion at the West Yamal shelf

Alexey Portnov[1,2], Jurgen Mienert[1], and Pavel Serov[1,2]

[1]CAGE - Centre for Arctic Gas Hydrate Environment and Climate, Department of Geology, UiT, Arctic University of Norway, Tromsø, Norway, [2]I.S. Gramberg VNIIOkeangeologia, Saint Petersburg, Russia

Abstract Thawing subsea permafrost controls methane release from the Russian Arctic shelf having a considerable impact on the climate-sensitive Arctic environment. Expulsions of methane from shallow Russian Arctic shelf areas may continue to rise in response to intense degradation of relict subsea permafrost. Here we show modeling of the permafrost evolution from the Late Pleistocene to present time at the West Yamal shelf. Modeling results suggest a highly dynamic permafrost system that directly responds to even minor variations of lower and upper boundary conditions, e.g., geothermal heat flux from below and/or bottom water temperature changes from above permafrost. Scenarios of permafrost evolution show a potentially nearest landward modern extent of the permafrost at the West Yamal shelf limited by ~17 m isobaths, whereas its farthest seaward extent coincides with ~100 m isobaths. The model also predicts seaward tapering of relict permafrost with a maximal thickness of 275–390 m near the shoreline. Previous field observations detected extensive emissions of free gas into the water column at the transition zone between today's shallow water permafrost (<20 m) and deeper water nonpermafrost areas (>20 m). The model adapts well to corresponding heat flux and ocean temperature data, providing crucial information about the modern permafrost conditions. It shows current locations of upper and lower permafrost boundaries and evidences for possible release of methane from the seabed to the hydrosphere in a warming Arctic.

1. Introduction

Studies of Pan-Arctic terrestrial and offshore permafrost evolution are becoming increasingly important for the interpretation of long term and recent rises of carbon gas emissions, and especially methane concentrations in both the ocean and atmosphere. Several hundred meter thick permafrost has been developed under low-temperature subaerial conditions during sea level lowstand of pre-Holocene regression (<21 ka). Permafrost existed in formerly drained areas of the Arctic sea shelves to present water depths of ~120 m below sea level (mbsl). Subsequent flooding of the Arctic shelves with relatively warm sea water, reaching 4–5°C at the seabed [*Miller et al.*, 2010], disturbed the thermodynamic balance within permafrost and provoked its melting. Such thawing permafrost conditions and associated release of methane have been previously studied in the Laptev and East Siberian Seas [*Danilov et al.*, 1998; *Hubberten and Romanovskii*, 2003; *Romanovskii et al.*, 2004; *Shakhova et al.*, 2010a]. High-resolution seismic data showing the subseabed and numerical modeling of the permafrost evolution suggest that permafrost is currently degrading over the East Siberian Arctic shelves, releasing significant amounts of methane through open taliks (local areas of thawed deposits within the permafrost) into the shallow seas and atmosphere [*Romanovskii et al.*, 2005; *Shakhova et al.*, 2013].

Subsea permafrost studies at the Canadian Beaufort Sea continental shelf [*Brothers et al.*, 2012; *Overduin et al.*, 2012; *Taylor et al.*, 2013] concentrated on analyses of raw seismic data [*Brothers et al.*, 2012] that indicate that subsea permafrost in the Canadian Beaufort Sea does not spread offshore beyond the 20 m isobaths. Subsea permafrost may also stimulate the development of shallow gas hydrates if the required temperature conditions for hydrate stability zone exist in the upper sedimentary cover [*Collett et al.*, 2011; *Romanovskii et al.*, 2005].

Only a few studies of subsea permafrost exist in the Kara Sea [*Portnov et al.*, 2013; *Rekant et al.*, 2005; *Rokos et al.*, 2001] and Pechora Sea [*Bondarev et al.*, 2002] that are confined to the interpretation of high-resolution seismic data. Multiple acoustic anomalies, discovered in the upper 30–50 m sediment section were associated with

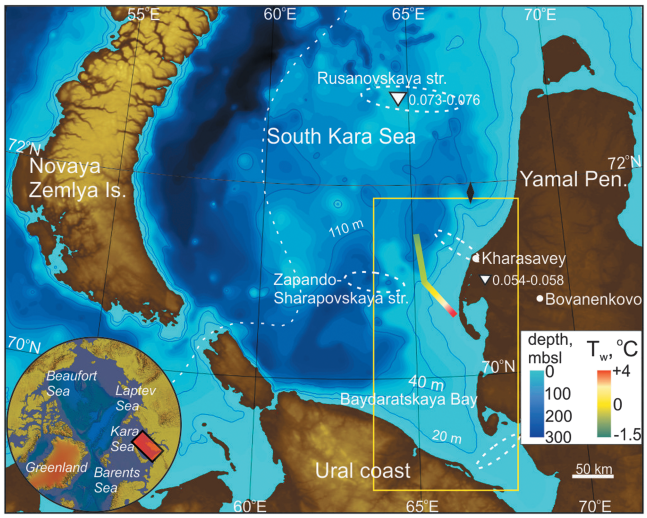

Figure 1. Bathymetric map of the South Kara Sea shelf. Yellow rectangle indicates the study area. Dashed white line shows the extent of the Last Glacial Maximum from the West, modified from *Polyak et al.* [2008]. White triangles show the heat flux values (W m^{-2}) onshore and offshore the Yamal Peninsula [*Khutorskoy and Podgornyh*, 2010]. Colored line shows the bottom water temperature (T_w) measured at the West Yamal shelf in August 2013. Dashed white oval lines show the sites where the offshore permafrost has been drilled [*GEOS*, 1997; *Melnikov and Spesivtsev*, 1995]. Black diamond shows the location of a gas seepage area chosen for gas-geochemical analyses of the sediments.

upward leakage of free gas from melting subsea permafrost [*Rokos et al.*, 2001]. *Rekant and Vasiliev* [2011] mapped the acoustic signatures of permafrost on seismic reflection data in the South Kara Sea suggesting that it extends to ~60 m isobath. At the West Yamal shelf, *Portnov et al.* [2013] documented extensive seafloor gas release from the seabed into the water column, in water depths ≥20 mbsl. The authors suggested that continuous subsea permafrost, extending offshore to 20 m isobaths, provided a seal through which gas cannot migrate.

Onshore drilling data from the Yamal Peninsula (Bovanenkovo and Kharasavey gas fields) revealed modern permafrost thickness ranging from ~250 to ~350 m [*Melnikov and Spesivtsev*, 1995; *Skorobogatov et al.*, 1998]. *Chuvilin et al.* [2000] indicated that intrapermafrost gas, revealed in drilling wells at the Bovanenkovo field, may result from both free gas accumulations and hydrate. Offshore drilling in the South Kara Sea revealed subsea permafrost at water depths 0–130 mbsl (Kharasavey structure, Baydaratskaya bay, Rusanovskaya, and Zapadno-Sharapovskaya structures, marked with dashed white ovals on Figure 1), though 85% of all drilled permafrost was discovered in the shallow (0–20 mbsl) water depths [*GEOS*, 1997; *Melnikov and Spesivtsev*, 1995]. However, such a high percentage of drilled shallow water permafrost may be misleading due to limited drilling data from deeper water areas.

There have been so far no comprehensive attempts to integrate modeling results of modern subsea permafrost in the Kara Sea with extensive high-resolution reflection seismic, heat flux, and ocean temperature data. Here we implement new 1-D modeling with the aim to study processes of permafrost evolution at the West Yamal shelf in space and time. The model simulates different scenarios of permafrost evolution for both Late Pleistocene and Holocene. Modeling results of present conditions are integrated with chirp data acquired during the cruise aboard the R/V *Neotrazimiy* (operated by I.S. Gramberg VNIIOkeangeologia in August and September 2012) to the West Yamal shelf. Based on the interpretation of these chirp data, *Portnov et al.* [2013] suggested that continuous ice-bearing subsea permafrost extends to at least 20 m isobaths. Incorporating both previously published chirp data and new modeling results, we reconstruct Late Pleistocene to present time evolution of permafrost from subaerial to subsea conditions over ~100 km distance from the present shoreline.

2. Geological Setting

South Kara Sea is bounded by the Novaya Zemlya Island in the west, and the Yamal Peninsula in the east. The shallow West Yamal shelf (<40 mbsl) extends to ~50–70 km offshore. It changes from gentle to steeper slopes seaward reaching 130–150 mbsl (Figure 1). Bottom water temperatures measured by VNIIOkeangeologia in August 2013 vary from +4°C in the narrow and shallow nearshore area (0–5 mbsl) to −1°C in water depths ≥40 m. The absence of major rivers on the Yamal Peninsula and the Ural coast exclude the impact of river and thus major freshwater discharge to the study area.

A thick sedimentary cover of the South Kara Sea basin overlies the Paleozoic basement. It is comprised of ~7–10 km thick Mesozoic and upper Cenozoic rocks. Being the offshore continuation of the West

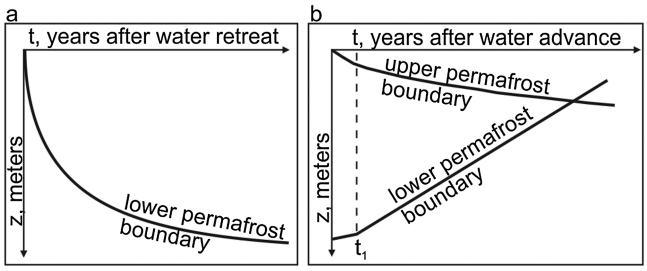

Figure 2. General curves describing generation of the (a) permafrost and its (b) degradation. The parameter t_1 specifies duration of the first stage of the permafrost degradation.

Siberian plate, the South Kara Sea basin comprises a rich hydrocarbon potential [*Stupakova*, 2011]. Conventional seismic data recovered multiple prospective structures with major potential for gas and gas condensate. South Kara Sea basin is characterized by elevated heat flux values at the West Yamal Peninsula ranging from 0.054–0.058 W m^{-2} onshore to 0.073–0.076 W m^{-2} offshore [*Khutorskoy and Podgornyh*, 2010].

Alternating periods of marine transgressions and regressions controlled Pleistocene-Holocene sedimentation processes. Upper sedimentary sections comprise marine and alluvial marine clays and silts, reaching 150–200 m thickness followed by a 5–20 m thick marine clay and sandy clay, and a 1–5 m thick Holocene clay, silt, and sand unit on top [*Melnikov and Spesivtsev*, 1995].

Reconstructions of the ice sheet extent suggest that the West Yamal shelf was last glaciated in the Early Weichselian (~90 ka), but it remains unclear whether the Middle Weichselian ice sheet (~60 ka) reached the study area [*Svendsen et al.*, 2004]. However, during the Last Glacial Maximum (LGM) (~21 ka), West Yamal shelf was not reached by an ice sheet [*Polyak et al.*, 2008].

3. Methods

We apply modeling techniques developed by *Sharbatyan* [1974] and adapted by *Melnikov and Spesivtsev* [1995] to reconstruct the evolution of permafrost during the glacial-interglacial periods. A similar approach was used by *Rokos et al.* [2009] to determine the thickness of permafrost on the shelves of Pechora and Kara Seas. Here we present mathematical equations to model and to estimate the generation and degradation of the permafrost at the West Yamal shelf.

3.1. Model of Subaerial Permafrost Generation

A model of permafrost generation estimates the time of permafrost thickness formation $t(z)$ in subaerial conditions during the regression of the sea by solving the following equation:

$$\frac{t}{t_0} = \frac{z}{z_0} + \ln\left(1 - \frac{z}{z_0}\right) \tag{1}$$

where t_o is the time (s) required for permafrost to reach ~84% of its potential thickness z_o.

$$z_0 = \frac{K_m(T_o - T_c)}{q} \tag{2}$$

where K_m is the thermal conductivity of frozen soil (W m^{-1} °C^{-1}), q is the heat flux (W m^{-2}), T_c is the mean ground air temperature during the regression (°C), and T_0 is the freezing temperature of the soil (°C).

$$t_0 = \frac{LdWz_0}{q} \tag{3}$$

where L is the latent heat of ice (J kg^{-1}), d is the density of wet sediment (kg m^{-3}), and W is water content (m^3 m^{-3}).

This model shows a lowering of the permafrost boundary with time after the ground temperature has dropped below the freezing point (Figure 2a). These conditions occur in the ice-free regions during a fast drainage of former subsea areas. The surface temperature of the sediment determines the upper boundary condition for the model, while geothermal heat flux, which is assumed to be constant with time, represents the lower boundary condition. This part of the model is used to calculate freezing of sediments.

Table 1. Basic Parameters Used for Modeling Permafrost Evolution on the West Yamal Shelf

Constant Parameters		Variables	
T_c (°C)	−15	T_w (°C)	−0.5
K_m (W m^{-1} °C^{-1})	1.39		+0.5
d (kg m^{-3})	1800		+1.5
–-L (J kg^{-1})	3.34 10^5	q (W m^{-2})	0.05
W (%)	30		0.06
T_0 (°C)	−1		0.07

3.2. Model of Subsea Permafrost Degradation

Our model of permafrost degradation defines the positions of upper and lower permafrost boundaries during interglacial periods, when former subaerial permafrost areas were flooded by transgressing ocean water masses. If the bottom water temperature is above the freezing temperature of the sediments, permafrost starts to thaw both from top to bottom, due to the geothermal heat flux (Figure 2b). According to *Sharbatyan* [1974], the process of permafrost degradation includes two stages. During the first stage, from transgression until time t_1, frozen sediment thickness expends its "cold reserves" leading to almost nongradient temperature distribution within the permafrost. The duration of the first stage is defined as

$$t_1 \simeq r t_0 \tag{4}$$

where coefficient $r = (T_w - T_0)/(T_0 - T_c)$ and T_w is the bottom water temperature, determining the upper boundary condition after flooding. The process of permafrost degradation from the top is approximated as follows:

$$z(t) = z_1 \frac{t_1}{t} \tag{5}$$

where $z_1 = (T_w - T_0)z_0/(T_w - T_c)$ is the maximum possible thickness of permafrost that can thaw from the top during the first stage. For the lower boundary the equation will be as follows:

$$z(t) = z_0 - \left(\frac{qt}{3LW}\right) \tag{6}$$

The second stage is characterized by more intensive permafrost degradation from the bottom. Ascent of the lower permafrost boundary is described by the following equation:

$$z(t) = z_1^{'} - \frac{qt}{LW} \tag{7}$$

where $z_1^{'} = z(t_1)$ is the depth of the lower permafrost boundary after the first stage. Lowering of the upper permafrost boundary during the second stage occurs noticeably slower, compared with the first stage and is described by the following relation:

$$z(t) \simeq z_0 \sqrt{\left(\frac{z_1}{z_0}\right)^2 + 2r\frac{t}{t_0 a}} \tag{8}$$

where a is the conductivity ratio of frozen to unfrozen sediments.

4. Input Parameters and Modeling Results of Permafrost Evolution

4.1. Input Parameters

The parameters used in the model are intentionally chosen to underestimate final results. This allows predicting minimum possible permafrost distributions and preserving the models flexibility while correlating modeling results with field data.

In our models we exclude existence of relict permafrost formed during preceding regression cycles, assuming that the upper sediment thickness at the West Yamal shelf was not frozen in the beginning of the last global sea level regression (~120 ka).

Various paleotemperature reconstructions of the ground surface show that from Early Weichselian onward, ground temperatures significantly varied in the Arctic. In the North Atlantic, relatively cold periods changed to short warm intervals, when the temperature rapidly increased by as much as 5–15°C [*Miller et al.*, 2010]. Analyses from exploration wells in the Canadian Arctic [*Taylor*, 1991] indicate average annual temperature

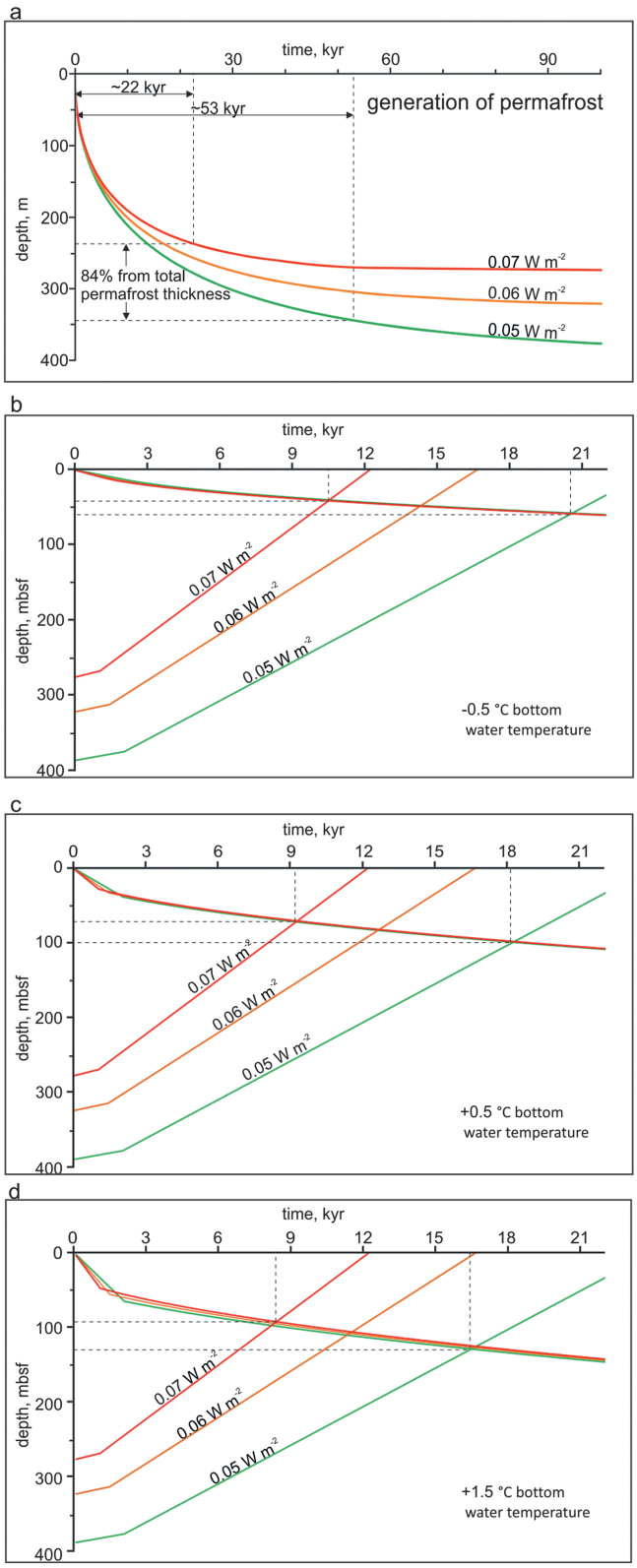

Figure 3

values as low as −15°C, but temperatures also varied from −10 to −20°C at the Yakutian coastal lowlands based on ice core records [*Gavrilov and Tumskoy*, 2003; *Romanovskii et al*., 2003]. Based on the sediment core data from the South Kara Sea, *Pavlidis et al*. [1998] concluded that Late Weichselian time was characterized by cold and dry climate with an annual air temperature as low as −20°C. Ground temperature in the permafrost regions is ~2–4°C warmer than the annual air temperature in these regions due to the snow cover, vegetation, and local geological and hydrological conditions. *Smith and Burgess* [2000] showed that at mean annual air temperatures from −15 to −20°C, mean annual ground temperatures vary in the range from ~ −12 to −18°C. Late Weichselian annual temperatures of the ground surface varied from −11 to −13°C at the latitude of the polar circle (~66.33°N) and from −15 to −18°C at northern Yamal and Gydan (~72°N) [*Rozenbaum and Shpolyanskaya*, 2000]. Therefore, we used an average surface temperature $T_c = -15$°C for the time of sea regression in our model.

To determine the bottom water temperature at the upper boundary, we used Arctic and Antarctic Research Institute (AARI) database, comprising the water temperature observations since the 1920s. We also used conductivity-temperature-depth measurements made by VNIIOkeangeologia in August 2013, which correspond well with AARI data set. Observations show that average annual bottom water temperature changes from +1°C at ~10 m water depth, to −0.5°C at 15–20 m water depth. The average temperature is −0.5°C and decreases with depth to −1°C at ~40 mbsl. As a consequence, we used for the upper boundary conditions three different values for bottom water temperature (−0.5, +0.5, and +1.5°C) and we used three different values for heat flux (0.05, 0.06, and 0.07 W m^{-2}) to determine the conditions at the lower boundary.

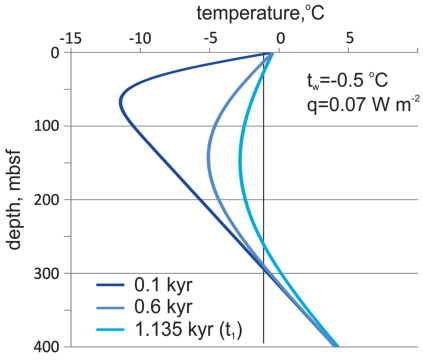

Figure 4. Leveling of the intrapermafrost temperature profile during the first stage t_1 after flooding. Geothermal heat flux and bottom water temperature are taken as 0.07 W m^{-2} and −0.5°C, respectively. A nearly nongradient temperature distribution inside the permafrost in ~1135 years after flooding indicates completion of stage t_1.

The term ice-bearing permafrost is used here to describe geological strata with temperatures ≤ −1°C. Freezing temperature of soils depends mainly on the grain size and salt content, which can vary on the West Yamal shelf. For clay and sandy clay of Baydaratskaya Bay with salt content 0.2–3.1%, freezing temperature differs in the range from −0.1 to −5.2°C [*GEOS*, 1997]. However, average prevailing NaCl salt content of 0.5–0.7% on the West Yamal shelf narrows the range of freezing temperature to approximately −1 to −1.5°C [*Brushkov*, 1998]. Using −1°C freezing temperature for our modeling does not allow defining local particularities of permafrost distribution, but it allows us to exclude majority of the deposits that may be in their transitional frozen-unfrozen state and thus to estimate regional distributions of soils with temperature ≤ −1°C.

Phase transition temperature for water (0°C) remains stable in the pressure range ~0.1–6 MPa [*Predel et al*., 2004], which refers to average lithostatic pressure at the depth interval ~0–300 m below the seafloor (mbsf) [*Bjørlykke et al*., 2005]. With increasing depths it slightly decreases reaching ~ −2°C at the depth of ~1000 mbsf. It allows the use of −1°C as a temperature boundary for permafrost in the upper ~500 m of the sediments, the depth interval of our modeling.

According to *GEOS* [1997] the upper sedimentary cover is comprised of clay and sandy clay with average density ~1800–1900 kg m^{-3} and water content ~30%. We applied the approximation of *Sass et al*. [1971] that the conductivity of a saturated rock is calculated depending on the conductivities of its compounds. We used thermal conductivity of grains ~1.1 W m^{-1} °C^{-1} and thermal conductivity of ice ~2.35 W m^{-1} °C^{-1}. The calculated value for our modeling exercise was ~1.39 W m^{-1} °C^{-1}. All the main input parameters for the models are given in Table 1.

For reconstructing sea level changes during Weichselian time we plotted the global eustatic sea level curve, using the open source database by *Lea et al*. [2003]. For the Holocene we used sea level reconstructions from *Fleming et al*. [1998] (Figure 7a). An estimation of the exposure and thus freezing time between regression and transgression provides various thicknesses of maximal permafrost. The different "subaerial" time spans for a particular bathymetric level govern the permafrost modeling results.

4.2. Modeling Results

Modeling results of permafrost generation show a maximum thickness of permafrost in subaerial conditions reaching ~390 m considering 0.05 W m^{-2} heat flux. It reduces to ~278 m if we increase the heat flux to 0.07 W m^{-2} (Figure 3a). The time required for generating ~84% of the permafrost is ~53 kyr and ~22 kyr using 0.05 and 0.07 W m^{-2}, respectively. After this time interval the interaction between external surface conditions (upper boundary condition) and geothermal heat flux (lower boundary condition) will tend to reach an equilibrium leading to a stable permafrost system until one of the boundary conditions is subject to change. The modeling results also suggest that ~60% of the entire permafrost thickness occurs during the first 10 kyr after the retreat of the sea and thus during terrestrial conditions.

The model also indicates that even a small variation in heat flux, surface air temperature, or water content may considerably change the total thickness of the permafrost. For example, a 1°C decrease of the surface air temperature will provoke a ~6–7% increase in the maximal possible permafrost thickness, demonstrating a highly dynamic permafrost system.

Figure 3. (a) Model of the permafrost generation, illustrating the dynamics of deep freezing of sediments under different geothermal heat flux conditions. Dotted lines define the time spans required to form ~84% of the total possible permafrost thickness. (b–d) Models of the permafrost degradation simulate the shift of upper and lower permafrost boundaries in time under various boundary conditions. Dotted lines define maximal and minimal time of the complete permafrost degradation and the subbottom depth where the permafrost ends.

Table 2. Time Spans Required for Total Degradation of Permafrost With Thickness z_0 Under Different Geothermal Heat Flux and Bottom Water Temperature[a]

Permafrost Degradation			
	T_w (°C)		
z_0 (m)/ q (W m^{-2})	−0.5	0.5	1.5
389/0.05	20.4 kyr (110 mbsl)	18.1 kyr (100 mbsl)	16.3 kyr (95 mbsl)
324/0.06	14.2 kyr (85 mbsl)	12.5 kyr (60 mbsl)	11.2 kyr (40 mbsl)
278/0.07	10.4 kyr (30 mbsl)	9.1 kyr (20 mbsl)	8.2 kyr (15 mbsl)

[a]In brackets are approximate water depths to which modern permafrost may extend.

Values obtained for the maximal permafrost thickness were respectively used to model the permafrost degradation (Figures 3b–3d). Duration of the first stage t_1, which is specific for nearly complete reduction of the vertical temperature gradient in the permafrost varies from ~1135 to ~2226 years given 0.07 W m^{-2} and 0.05 W m^{-2} heat flux, respectively. The dynamics of the temperature leveling inside the permafrost during stage t_1, i.e., after flooding is shown in Figure 4.

During the second stage, at low bottom water temperatures (~ − 0.5 to −1°C), the geothermal heat flux makes the most significant contribution to permafrost degradation while thawing from the top of the permafrost goes considerably slow, and its rate slightly decreases with time. Given a heat flux of 0.05 W m^{-2}, the lower and upper permafrost boundaries will merge after about 20.4 kyr after flooding. Noteworthy, it takes only half of the time (i.e., ~10.2 kyr) for total permafrost degradation, using 0.07 W m^{-2} heat flux. The lower and upper boundaries start to merge in the interval ~47–60 mbsf if the bottom water temperature is −0.5°C (Figure 3b). Raised bottom water temperatures result in a faster reduction of the upper permafrost

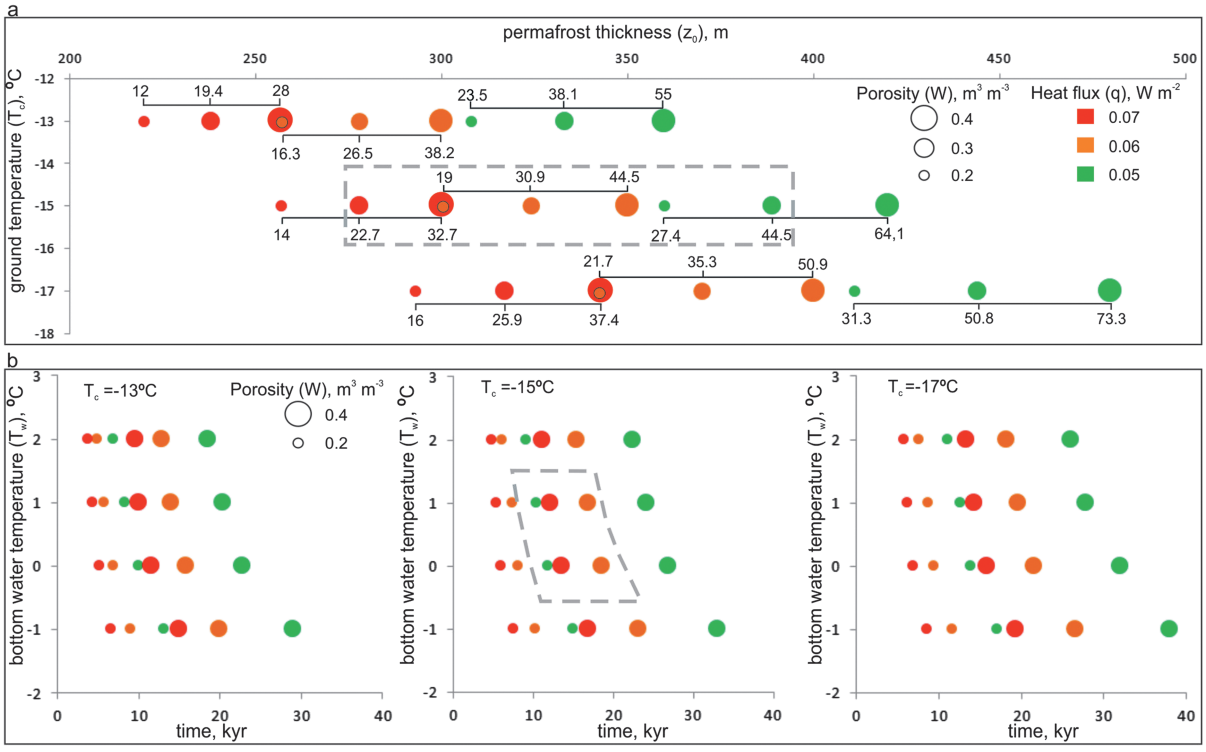

Figure 5. Sensitivity analyses for permafrost generation and permafrost degradation models. (a) Variation of the maximal potential permafrost thickness z_0 in relation to the annual ground temperature (T_c), porosity of the sediments (W), and geothermal heat flux (q). Numbers at the rounds show the time spans (kyr) required for generation of z_0 under certain input parameters. (b) Sensitivity analysis showing the difference in the time of total permafrost degradation under changing bottom water temperature (T_w), porosity of the sediments, and geothermal heat flux. Analysis is performed for three scenarios, considering different annual ground temperatures during permafrost generation stage, as shown in Figure 5a. Dashed gray polygons on Figures 5a and 5b indicate the approximate model space where we fit our calculations based on the input parameters appropriate for the West Yamal shelf.

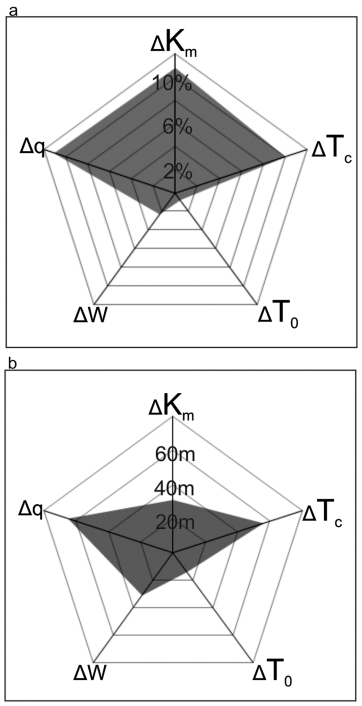

Figure 6. (a) Percentage change of the total permafrost thickness after the alternate change of one of the input parameters by 10%. (b) Change of the total permafrost thickness in meters after alternate change of one of the parameters by the following values: $\Delta K_m = 0.1\ \mathrm{W\,m^{-1}\,°C^{-1}}$, $\Delta T_c = 2°\mathrm{C}$, $\Delta T_0 = 0.5°\mathrm{C}$, $\Delta W = 0.1\ \mathrm{m\,m^{-3}}$, and $\Delta q = 0.01\ \mathrm{W\,m^{-2}}$.

boundary, especially during the first melting stage t_1 (Figures 3c and 3d). Given a +1.5°C bottom water temperature, the permafrost will completely degrade in ~16.1 kyr with $0.05\ \mathrm{W\,m^{-2}}$ and in ~8.2 kyr with $0.07\ \mathrm{W\,m^{-2}}$ heat flux. The lower and upper boundaries will merge at an approximate depth interval of 95–128 mbsf. Table 2 shows the time periods required for complete degradation of subsea permafrost using different boundary conditions.

4.3. Sensitivity Analysis

Chosen input parameters allow modeling likely scenarios of subsea permafrost evolution on the West Yamal shelf. Sensitivity analysis shows how chosen input parameters modify the range of the potential solutions. Figure 5a illustrates how the maximal potential permafrost thickness z_0 depends on the changing ground temperature T_c (−13, −15, and −17°C), porosity of the sediments W (0.2, 0.3, and $0.4\ \mathrm{m^3\,m^{-3}}$), and geothermal heat flux q (0.05, 0.06, and $0.07\ \mathrm{W\,m^{-2}}$). Each separate run of the model gives a result depending on the combination of the input parameters. Sensitivity analysis predicts that at the warmest boundary conditions ($T_c = -13°\mathrm{C}$ and $q = 0.07\ \mathrm{W\,m^{-2}}$), z_0 varies in the range of ~217–255 m (Figure 5a) depending on the porosity, whereas coldest boundary conditions ($T_c = -17°\mathrm{C}$ and $q = 0.05\ \mathrm{W\,m^{-2}}$) result in z_0 ~405–478 m depending on the porosity. The time period of z_0 thickness formation under these conditions changes from ~12 kyr to 73.3 kyr (Figure 5a). Note that a different combination of input parameters may result in similar z_0 and t_0. The uncertainty of the model for permafrost generation is approximately 10 m.

Figure 5b demonstrates how the different combinations of T_c, W, q, and T_w affect the time of complete thawing of the permafrost thickness. It shows that doubling of sediment porosity, but holding the other parameters constant, leads to more than a twice longer period of total permafrost degradation. The effect from the change of the geothermal heat flux is predictably higher at the lower bottom water temperatures, because in these conditions it is almost solely responsible for permafrost melting. The chosen diapason of input parameters results in a time of total permafrost degradation, changing in the range from ~4 to 38 kyr. Dashed gray polygons on Figures 5a and 5b indicate the approximate model space where we fit our calculations based on the used input parameters for the West Yamal shelf. The uncertainty of the model for permafrost degradation is approximately 100 years.

We also analyzed which of the input parameters has the most significant effect on the model. First, we changed each of the input parameters by 10% and explored how the total permafrost thickness z_0 changed, in percent from its initial value (Figure 6a). We also designed a similar chart, which was not based on the percentage change, but on the same variation of the input parameters that we used for the previous sensitivity model ($\Delta K_m = 0.1\ \mathrm{W\,m^{-1}\,°C^{-1}}$, $\Delta T_c = 2°\mathrm{C}$, $\Delta T_0 = 0.5°\mathrm{C}$, $\Delta W = 0.1\ \mathrm{m\,m^{-3}}$, $\Delta q = 0.01\ \mathrm{W\,m^{-2}}$). This chart showed how z_0 changes in meters (Figure 6b). Both charts revealed that heat flux and initial ground temperature most significantly change the total permafrost thickness, whereas freezing temperature of the sediments and porosity change led to only minor variations of z_0.

5. Interpretation and Discussions

5.1. Eustatic Sea Level Change and Evolution of the Permafrost at the West Yamal Shelf

Our results provide information about the present approximate extent of permafrost at the West Yamal shelf. The time periods when the current seabed was exposed to freezing and subsequent thawing of permafrost relates directly to sea level variations in the study area. Apart from global sea level variations,

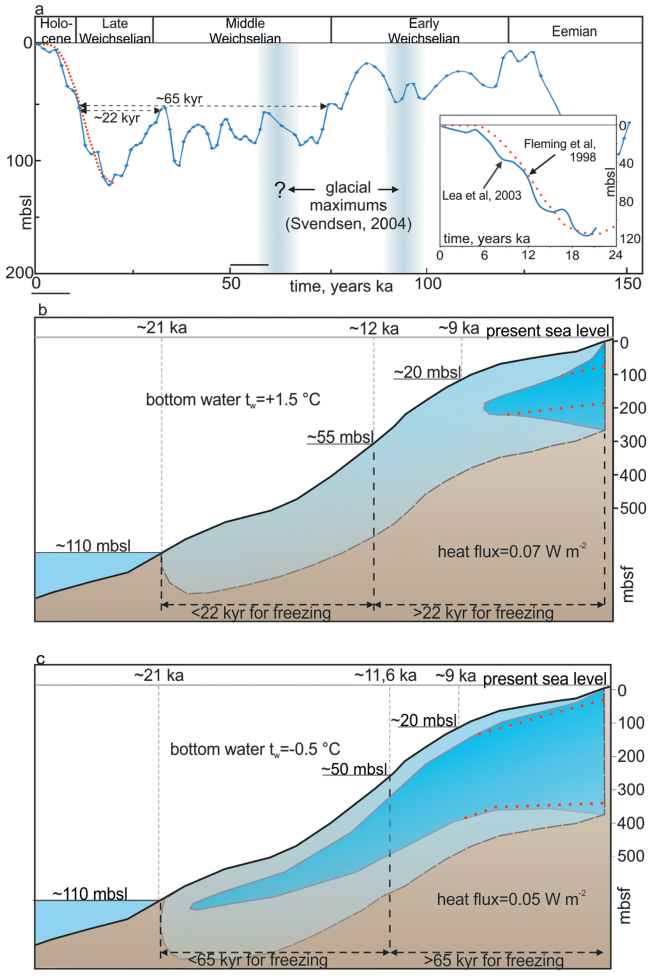

Figure 7. (a) Eustatic sea level curves, used to define the exposure and thus freezing time for particular bathymetric levels at the West Yamal shelf. *Lea et al.* [2003]—blue line, *Fleming et al.* [1998]—red-dotted line. (b) Minimum and (c) maximum permafrost scenarios at the West Yamal shelf show the extent of the permafrost during the regression (light blue) and after the transgression (dark blue). Red-dotted lines within the dark blue areas show the alternative location of the permafrost boundaries related to the high sea level conditions during the last ~5 kyr. Note the different subsea and subseabed vertical scales.

regional vertical tectonic and glacio-isostatic movements may provide additional factors influencing sea level change in each particular region.

As part of the South Kara Sea, the West Yamal shelf did not undergo significant tectonic movements during the Weichselian [*Pavlidis et al.*, 1998]. Modern and detailed tectonic movements of West Yamal are not very well constrained. According to *Pavlidis et al.* [1998], existing estimates vary from 0.04 cm/yr subsidence to 0.4 cm/yr uplift. Although the southern Kara Sea was not glaciated during the Late Weichselian (LGM ~21 ka) [*Polyak et al.*, 2008], the study area may have been affected by small glacio-isostatic vertical movements, reaching tens of meters in adjacent areas of the northwestern Barents Sea [*Forman et al.*, 2004; *Peltier*, 1996]. However, according to these authors the impact from such motions on the West Yamal shelf was insignificant. Based on high-resolution seismic data, *Musatov* [1998] mapped distinct erosional surfaces of the LGM, indicating the last sea level regression in the study area. The mapped erosional surface exists today in water depths ~120 mbsl, corresponding well with the last global sea level low stand [*Fleming et al.*, 1998]. Therefore, tectonic and glacio-isostatic movements of the West Yamal shelf during the Weichselian are most likely negligible.

It remains unclear whether the Middle Weichselian glaciation (~60 ka) had an impact on the West Yamal shelf [*Svendsen et al.*, 2004] (Figure 7a). An impact would be in any case minor because the major permafrost thickness would have been reached already in ≤53 kyr even at low heat flux (0.05 W m^{-2}) (Figure 3a). Given these time constraints, we applied the global sea level curve for the modeling of permafrost at the West Yamal shelf.

Figures 7b and 7c represent two scenarios of subsea permafrost evolution on the West Yamal shelf. The models simulate relict permafrost generation and degradation using maximum and minimum boundary conditions (geothermal heat flux and bottom water temperature).

5.2. Minimum Continuous Permafrost Scenario: 0.07 W m^{-2} Geothermal Heat Flux and +1.5°C Bottom Water Temperature

According to the modeling results of permafrost generation, the permafrost system tends to become thermodynamically stable after ~22 kyr considering constant freezing from the top and geothermal heat flux of 0.07 W m^{-2}, which results in a maximal possible permafrost thickness of ~280 m (Figure 3a). Vast areas of the West Yamal shelf shallower than 55 m were exposed to freezing conditions of more than 22 kyr

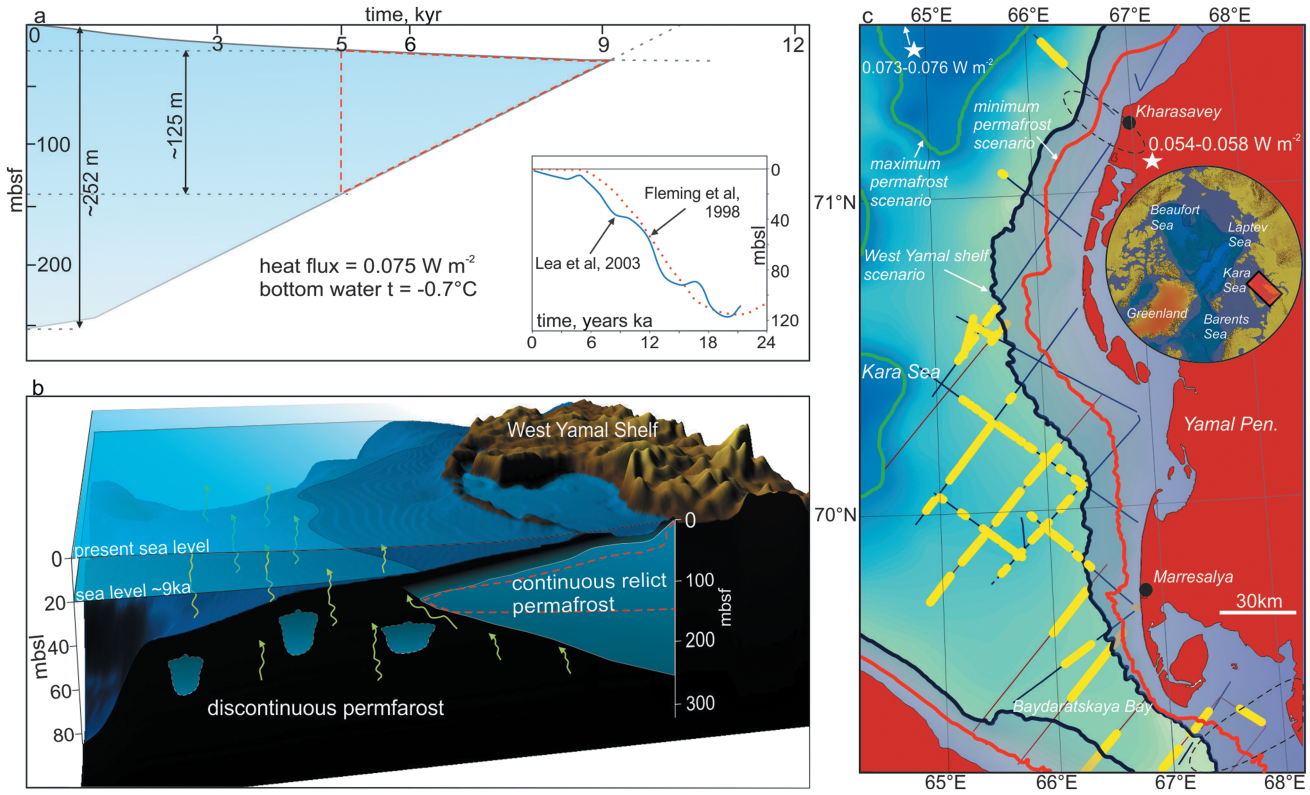

Figure 8. (a) Proposed modeled scenario of the permafrost degradation at the West Yamal shelf. Blue area corresponds to gradual rise of the sea level during Holocene. Red-dashed lines in Figures 8a and 8b show the alternative location of the permafrost boundaries, if the sea reached its modern level at ~5 ka and remained stable until the present time. (b) Conceptual model of the West Yamal shelf, showing modern extent of continuous relict subsea permafrost based on the modeling results and the evidence of free gas expulsion recorded previously in the water column [*Portnov et al.*, 2013]. We suppose that discontinuous patches of permafrost may still exist in the water depths >20 m. Note the different subsea and subseabed vertical scales. (c) Green and red lines show the maximal and minimal modeled extent of the permafrost at the West Yamal shelf, respectively. Yellow lines show the distribution of gas flares in the water column [*Portnov et al.*, 2013], dashed black ovals indicate the areas where permafrost has been drilled [*GEOS*, 1997]. White stars indicate measured geothermal heat flux [*Khutorskoy and Podgornyh*, 2010].

(Figures 7a and 7b). The time span for freezing at deeper water depths was shorter because of the reduced time period between the retreat and subsequent advance of the sea. As a result, it creates thinner total permafrost beneath the submerged parts of the shelf (~55–120 mbsl). A bottom water temperature of +1.5°C and 0.07 W m^{-2} heat flux suggest a total degradation of former terrestrial permafrost in 8.2 kyr (Figure 3d), indicating that relict subsea permafrost may currently exist only in regions flooded less than 8.2 ka. According to eustatic sea level reconstructions, this time period corresponds to water depths ≤17 mbsl (Figures 7a, 7b, and, 8c).

5.3. Maximum Continuous Permafrost Scenario: 0.05 W m^{-2} Geothermal Heat Flux and −0.5°C Bottom Water Temperature

Using the lower boundary conditions, the maximum time for the permafrost formation reaches ~53 kyr. Eustatic sea level reconstructions show that only West Yamal shelf, shallower than ~50 m, has undergone continuous subaerial freezing for more than 53 kyr (Figure 7a). These areas were exposed to deep freezing conditions reaching up to ~390 mbsf (Figure 3a). According to our model, permafrost in deeper water shelf regions (~50–120 mbsl) had lower permafrost thickness. These areas were continuously drained for a shorter time period, but still, it enabled freezing from the seafloor to a depth of ~270 mbsf. As shown above, lower heat flux and lower bottom water temperatures significantly decrease the rate of permafrost degradation during the time of sea level rise (Figure 3b), indicating that subsea permafrost can still exist today at water depths as deep as ~100 m (Figures 7c and 8c).

Using eustatic sea level reconstructions, the modeling results provide locations of both upper and lower permafrost boundaries at a particular water depth. Modern boundaries of subsea permafrost, designated on

Figures 7b and 7c as gray solid lines, correspond to continuous and gradual sea level rise during the last sea level transgression. According to *Fleming et al*. [1998], the sea level reached its present position ~5 ka and remained relatively stable until the present time (inset of Figure 7a). In such a scenario, upper and lower permafrost boundaries should move closer within the nearshore area, noticeably reducing the total permafrost thickness (red-dotted lines on Figures 7b and 7c).

Our modeling results show a highly dynamic permafrost system where even a small change in geothermal heat flux and/or bottom water temperature can significantly change the positions of lower and upper permafrost boundaries. The dynamics are less significant if changes in thermal conductivity and/or density occur. Based on our modeling results we propose a most likely scenario for the evolution of permafrost at West Yamal shelf.

5.4. West Yamal Shelf Scenario

Previous studies have shown an intensive and continuous escape of free gas in the water column at the area of the West Yamal shelf [*Portnov et al*., 2013]. Seabed gas expulsions form a front of flares limited by the 20 m isobaths that is completely disappearing at shallower water depths. This pattern and related process appear to be controlled by continuous subsea permafrost, which extends offshore to ~20 m isobaths, creating a seal through which gas cannot migrate.

According to *GEOS* [1997], about 85–90% of all permafrost drilled in the Kara Sea and 100% of the permafrost drilled in Baydaratskaya Bay were found within water depths 0.5–20 m. Moreover, about 94% of all permafrost drilled in the Kara Sea and 92% drilled in Baydaratskaya Bay were found within a distance of 0.2–20 km from the shoreline. In more than 50% of drilled permafrost, the upper permafrost boundary existed at subbottom depths 15–25 m [*GEOS*, 1997]. However, the data provide only approximate information due to the irregular grid of wells in the Kara Sea but, together with modeling results, it allows to significantly reduce the uncertainties for the depth intervals where permafrost exists.

Based on previous field studies [*Portnov et al*., 2013], the present extent of continuous relict permafrost at the West Yamal shelf is limited by ~20 m isobaths. Reconstructions of eustatic sea level change during the Holocene in the region indicate that 20 m isobaths matches with 9 ka, suggesting that permafrost has degraded in the previously flooded areas. Sensitivity analysis indicates that a time span of 9 kyr for the total degradation of permafrost may be obtained using different combinations of input parameters (Figure 5b). Figure 8a shows modeling results that suggest such a scenario by changing upper and lower boundary conditions, but leaving porosity and ground temperature values constant, appropriate for the West Yamal shelf ($W = 30\%$, $T_c = -15°C$). Heat flux $<0.07\ W\ m^{-2}$ requires to input average bottom water temperatures $> +1.5°C$, which are apparently too high for the study area. We therefore favor model input parameters, using an elevated heat flux but lower bottom water temperatures. Here we used $0.075\ W\ m^{-2}$ heat flux, which is consistent with the available information from the South Kara Sea [*Khutorskoy and Podgornyh*, 2010] and $-0.7°C$ average bottom water temperature. These input parameters provide an age for the total permafrost degradation of ~9 kyr. Considering the uncertainties in the sea level history during the last ~5 kyr, we introduced two alternative conceptual models with chosen input parameters. The first model is based on the assumption that the sea level raised gradually, which resulted in a maximum thickness of modern subsea permafrost (~252 m) proximal to the shoreline (Figures 8a and 8b). The upper permafrost boundary is slowly descending seaward, reaching ~30 mbsf at 15–20 m water depths. Discontinuous permafrost formations may still exist at deeper water depths, where they have been also documented by drilling [*Melnikov and Spesivtsev*, 1995]. The second model considers that the sea level reached its present position at ~5 ka and remained relatively stable since then. In this case the maximal permafrost thickness decreases to ~125 m, indicating that the permafrost had enough time to degrade significantly even at shallow areas of the West Yamal shelf (Figures 8a and 8b). In this case the upper permafrost boundary is abruptly submerging to subbottom depth of ~20 mbsf within a narrow corridor of the nearshore area. It gently descends seaward where it ends at ~30 mbsf. Our model does not consider the Holocene climatic optimum when the annual air temperatures could exceed modern temperatures by ~3–5°C [*Pavlidis et al*., 1998] and provoke warming of the bottom water masses in the shallow nearshore area. However, this could cause even more intensive melting of the permafrost from the upper boundary and thus result in formation of alongshore taliks as described by *Rekant and Vasiliev* [2011].

Our results present likely scenarios supported by both modeling and observations of the relict subsea permafrost evolution at the West Yamal shelf (Figure 8). The areas have been affected particularly during

the final phase of sea level transgression, when sea level slowly encroached landward, eroding the shoreline. This caused a more rapid and uneven thawing of the upper permafrost surface during the first stage of the permafrost degradation, determining an abrupt and indented topography of the upper permafrost boundary.

5.5. Origin of Seeping Gas

It is still under discussion whether permafrost creates a completely impermeable seal which hinders any gas to migrate upward or it may contain local areas of reduced permeability with focused and/or increased methane release. *Shakhova et al*. [2010b] suggest that permafrost is not permeable for gas, while *Yakushev* [2009] suggests the existence of both scenarios depending on the geological evolution of a region. It is essential to realize that permeability depends on the lithological properties, water content, ice content, and geological structure of the sediment formation [*Yakushev*, 2009]. We suppose that frozen deposits at the West Yamal shelf are much less permeable for gas than for nonfrozen sediments, thus allowing trapping free gas beneath or inside the permafrost. We suggest that gas bubbles observed on the chirp data may also originate from the modern transformation of cryotic sediments, i.e., from frozen to unfrozen state. Gas formerly trapped within the permafrost may escape and ascend from the melting sediments to the water column in water depths >20 mbsl. Results of gas-geochemical analyses made by VNIIOkeangeologia indicate that gas, reaching the upper sediment cover, is mainly biogenic in origin. Samples of gas from gravity cores, which were recovered in gas seepage spot at the West Yamal shelf (Figure 1), contain very high concentrations of methane (up to 1176 μmol). Ratio of methane to the sum of its homologues ($C_1/C_2 - C_5 \geq 3000$) indicates a predominantly biogenic source for hydrocarbon gases. Methane $\delta^{13}C$ ratio ranged from −77.8‰ to −79.9‰ and δD ranged from −270.1‰ to −289.4‰ support its microbial origin, which is somewhat surprising in an area of known occurrences of deep hydrocarbon provinces [*Stupakova*, 2011].

6. Conclusions

The model shows the evolution of the relict subsea permafrost at the West Yamal shelf for the Late Pleistocene-Holocene. Modeling results using upper and lower boundary conditions suggest maximum and minimum scenarios for modern permafrost existence. Maximum permafrost shows at 0.05 W m^{-2} heat flux and −0.5°C bottom water temperature, which provides for a long-term (~20.4 kyr) conservation of relict subsea permafrost. It would show its modern extent to ~100 m isobaths with a maximal thickness ~390 m. Minimum permafrost occurs at 0.07 W m^{-2} heat flux and +1.5°C bottom water temperature. These conditions result in a complete degradation of the permafrost in only ~8.2 kyr, suggesting that its modern extent is limited to ~17 m isobaths. Maximum thickness reaches only ~275 m, which is ~115 m less compared to maximum permafrost scenario. Reconstructions of the sea level history, determining the duration of subaerial and subsea conditions are essential for precise modeling of the permafrost evolution. Previously documented gas expulsions from the seabed together with modeling results support a scenario for the West Yamal shelf in which permafrost with its maximal nearshore thickness ~250 m tapers seaward and ends at ~20 m isobaths. This scenario occurs at elevated (0.075 W m^{-2}) heat flux and average bottom water temperature of −0.7°C. In deeper water depths, patches of permafrost may still exist but it does not create an impermeable seal for gas. Gas-geochemical analyses reveal extremely high methane concentrations (up to 1176 μmol) of microbial origin.

Acknowledgments
The research is part of the Centre of Excellence: Arctic Gas Hydrate, Environment and Climate (CAGE) funded by the Norwegian Research Council (grant 223259). A. Portnov is supported by a Statoil fellowship through the University of Tromsø. The field research was funded by the Federal Subsoil Resources Management Agency of Russia (object 70–113: "Regional geologic-geophysical explorations at Yamal sector of South Kara Sea shelf"). We thank A. Vasiliev, the anonymous reviewer and Editor-in-Chief Dennis Baldocchi for substantial and constructive comments. All questions regarding access to the data are to be sent to Alexey Portnov (portnovalexey@gmail.com).

References

Bjørlykke, K., K. Høeg, J. I. Faleide, and J. Jahren (2005), When do faults in sedimentary basins leak? Stress and deformation in sedimentary basins; examples from the North Sea and Haltenbanken, offshore Norway, *AAPG Bull.*, *89*(8), 1019–1031, doi:10.1306/04010504118.

Bondarev, V., S. Rokos, D. Kostin, A. Dlugach, and N. Polyakova (2002), Underpermafrost accumulations of gas in the upper part of the sedimentary cover of the Pechora Sea, *Geol. Geophys.*, *43*(7), 587–598.

Brothers, L. L., P. E. Hart, and C. D. Ruppel (2012), Minimum distribution of subsea ice-bearing permafrost on the U.S. Beaufort Sea continental shelf, *Geophys. Res. Lett.*, *39*, L15501, doi:10.1029/2012GL052222.

Brushkov, A. V. (1998), *Saline Permafrost of the Arctic Coast, Their Origin and Engineer-Geological Particularities*, 331 pp., Moscow State Univ., Moscow.

Chuvilin, E. M., V. S. Yakushev, and E. V. Perlova (2000), Gas and possible gas hydrates in the permafrost of Bovanenkovo gas field, Yamal peninsula, West Siberia, *Alfred Wegener Inst. Polar Mar. Res. German Soc. Polar Res.*, *68*, 215–219.

Collett, T. S., M. W. Lee, W. F. Agena, J. J. Miller, K. A. Lewis, M. V. Zyrianova, R. Boswell, and T. L. Inks (2011), Permafrost-associated natural gas hydrate occurrences on the Alaska North Slope, *Mar. Pet. Geol.*, *28*(2), 279–294, doi:10.1016/j.marpetgeo.2009.12.001.

Danilov, I. D., I. Komarov, and A. Vlasenko (1998), Pleistocene-Holocene permafrost of the East Siberian Eurasian Arctic shelf, in *PERMAFROST-Seventh International Conference*, Collection Nordicana No. 55., pp. 207–212, Yellowknife.
Fleming, K., P. Johnston, D. Zwartz, Y. Yokoyama, K. Lambeck, and J. Chappell (1998), Refining the eustatic sea-level curve since the Last Glacial Maximum using far- and intermediate-field sites, *Earth Planet. Sci. Lett.*, *163*(1–4), 327–342, doi:10.1016/S0012-821X(98)00198-8.
Forman, S. L., D. J. Lubinski, Ó. Ingólfsson, J. J. Zeeberg, J. A. Snyder, M. J. Siegert, and G. G. Matishov (2004), A review of postglacial emergence on Svalbard, Franz Josef Land and Novaya Zemlya, northern Eurasia, *Quat. Sci. Rev.*, *23*(11–13), 1391–1434, doi:10.1016/j.quascirev.2003.12.007.
Gavrilov, A. V., and V. E. Tumskoy (2003), Model of mean annual temperature history for the Yakutian coastal lowlands and Arctic shelf during the last 400 thousand years, paper presented at 8th, International conference on permafrost, Zürich, Switzerland.
GEOS (1997), Baydaratskaya Bay environmental conditions. The basic result of studies for the pipeline "Yamal-Center" underwater crossing design., 432 pp., GEOS, EPS "Eco-System library", Moscow.
Hubberten, H. W., and N. N. Romanovskii (2003), The main features of permafrost in the Laptev Sea region, Russia, in *8th International Conference on Permafrost*, pp. 431–436, Balkema, Zürich, Switzerland.
Khutorskoy, M. D., and L. V. Podgornyh (2010), Geothermics of the Arctic basin—The problems and solutions. Geothermal field and the Arctic shelf oil and gas bearing, *Monit. Sci. Technol.*, *1*(1), 6–26.
Lea, D. W., P. A. Martin, D. K. Pak, and H. J. Spero (2003), *350 KYr Sea Level Reconstruction and Foraminifer Isotope Data*, edited by I. P. W. D. C. A. f. Paleoclimatology and D. C. S. #2003-010, NOAA/NGDC Paleoclimatology Program, Boulder, Colo.
Melnikov, V., and V. Spesivtsev (1995), Engineering-geological conditions of Barents and Kara Sea shelves.
Miller, G. H., et al. (2010), Temperature and precipitation history of the Arctic, *Quat. Sci. Rev.*, *29*(15–16), 1679–1715, doi:10.1016/j.quascirev.2010.03.001.
Musatov, E. (1998), Structure of Cenozoic sedimentary cover and neotectonics of the Barents-Kara Sea shelf based on high-resolution seismic data, *Russ. J. Earth Sci.*, *1*(2), 157–183.
Overduin, P. P., S. Westermann, K. Yoshikawa, T. Haberlau, V. Romanovsky, and S. Wetterich (2012), Geoelectric observations of the degradation of nearshore submarine permafrost at Barrow (Alaskan Beaufort Sea), *J. Geophys. Res.*, *117*, F02004, doi:10.1029/2011JF002088.
Pavlidis, Y. A., A. S. Ionin, F. A. Sherbakov, N. N. Dunaev, and S. L. Nikiforov (1998), *The Arctic Shelf. Late-Quaternary Geological History as a Framework for the Future Prognosis*, pp. 184, GEOS, Moscow.
Peltier, R. W. (1996), Mantle viscosity and ice-age ice sheet topography, *Science*, *273*, 1359–1364.
Polyak, L., F. Niessen, V. Gataullin, and V. Gainanov (2008), The eastern extent of the Barents–Kara ice sheet during the Last Glacial Maximum based on seismic-reflection data from the eastern Kara Sea, *Special issue*: *Arctic Palaeoclimate and its Extremes* (*APEX*), *Polar Res.*, *27*(2), 162-174, doi:10.1111/j.1751-8369.2008.00061.x.
Portnov, A., A. J. Smith, J. Mienert, G. Cherkashov, P. Rekant, P. Semenov, P. Serov, and B. Vanshtein (2013), Offshore permafrost decay and massive seabed methane escape in water depths >20m at the South Kara Sea shelf, *Geophys. Res. Lett.*, *40*, 3962–3967, doi:10.1002/grl.50735.
Predel, B., M. Hoch, and M. Pool (2004), *Phase Diagrams and Heterogeneous Equilibria*, 349 pp., Springer, Berlin.
Rekant, P., and A. Vasiliev (2011), Distribution of subsea permafrost at the Kara Sea shelf, *Cryosphere Earth*, *XV*(4), 69–72.
Rekant, P., G. Cherkashev, B. Vanstein, and P. Krinitsky (2005), Submarine permafrost in the nearshore zone of the southwestern Kara Sea, *Geo-Mar. Lett.*, *25*(2–3), 183–189, doi:10.1007/s00367-004-0199-5.
Rokos, S., D. Kostin, and A. Dlugach (2001), Free gas and permafrost in the upper deposits of shallow areas at Pechora and Kara Sea shelf, *Sediment. Processes Mar. Ecosyst. Evol. Mar. Periglacial Conditions*, 40–51, 256.
Rokos, S., A. Dlugach, A. Loktev, D. Kostin, and S. Kulikov (2009), Permafrost of the Pechora and the Kara Seas: Genesis, structure and conditions of its distribution, *Eng Surv.*, *10*, 38–41.
Romanovskii, N. N., H. W. Hubberten, V. E. Romanovsky, and A. L. Kholodov (2003), Permafrost evolution under the influence of long-term climate fluctuations and glacio-eustatic sea-level variation: Region of Laptev and East Siberian Seas, Russia, paper presented at 8th International Conference on Permafrost, Swets & Zeitlinger, Zurich, Switzerland.
Romanovskii, N. N., H. W. Hubberten, A. V. Gavrilov, V. E. Tumskoy, and A. L. Kholodov (2004), Permafrost of the east Siberian Arctic shelf and coastal lowlands, *Quat. Sci. Rev.*, *23*(11–13), 1359–1369, doi:10.1016/j.quascirev.2003.12.014.
Romanovskii, N. N., H. W. Hubberten, A. V. Gavrilov, A. A. Eliseeva, and G. S. Tipenko (2005), Offshore permafrost and gas hydrate stability zone on the shelf of East Siberian Seas, *Geo-Mar. Lett.*, *25*(2–3), 167–182, doi:10.1007/s00367-004-0198-6.
Rozenbaum, G., and N. Shpolyanskaya (2000), *Late Cenozoic History of Arctic Permafrost and Tendency of its Evolution*, Scientific World, Moscow.
Sass, J. H., A. H. Lachenbruch, and R. J. Munroe (1971), Thermal conductivity of rocks from measurements on fragments and its application to heat-flow determinations, *J. Geophys. Res.*, *76*(14), 3391–3401, doi:10.1029/JB076i014p03391.
Shakhova, N., I. Semiletov, I. Leifer, A. Salyuk, P. Rekant, and D. Kosmach (2010a), Geochemical and geophysical evidence of methane release over the East Siberian Arctic Shelf, *J. Geophys. Res.*, *115*, C08007, doi:10.1029/2009JC005602.
Shakhova, N., I. Semiletov, A. Salyuk, V. Yusupov, D. Kosmach, and Ö. Gustafsson (2010b), Extensive methane venting to the atmosphere from sediments of the East Siberian Arctic shelf, *Science*, *327*, 1246–1250.
Shakhova, N., et al. (2013), Ebullition and storm-induced methane release from the East Siberian Arctic shelf, *Nat. Geosci.*, *7*(1), doi:10.1038/ngeo2007.
Sharbatyan, A. A. (1974), *Extremal Estimates in Geothermy and Geocryology*, Nauka, Moscow.
Skorobogatov, V. A., V. S. Yakushev, and E. M. Chuvilin (1998), Sources of natural gas within permafrost North-West Siberia, paper presented at 7th International Conference on permafrost, Canada.
Smith, S., and M. Burgess (2000), Ground temperature database for Northern Canada, *Geol. Surv. of Can., Open File Rep. 3954,* 28 pp.
Stupakova, A. (2011), Structure and petroleum potential of the Barents-Kara Shelf and adjacent territories, *Oil Gas Geol.*, *6*, 99–115.
Svendsen, J. I., et al. (2004), Late Quaternary ice sheet history of northern Eurasia, *Quat. Sci. Rev.*, *23*(11–13), 1229–1271, doi:10.1016/j.quascirev.2003.12.008.
Taylor, A. E. (1991), Marine transgression, shoreline emergence: Evidence in seabed and terrestrial ground temperatures of changing relative sea levels, Arctic Canada, *J. Geophys. Res.*, *96*(B4), 6893–6909, doi:10.1029/91JB00293.
Taylor, A. E., S. R. Dallimore, P. R. Hill, D. R. Issler, S. Blasco, and F. Wright (2013), Numerical model of the geothermal regime on the Beaufort Shelf, arctic Canada since the Last Interglacial, *J. Geophys. Res. Earth Surface*, *118*, 2365–2379, doi:10.1002/2013JF002859.
Yakushev, V. S. (2009), *Natural Gas and Gas Hydrates in the Permafrost*, 192 pp., GAZPROM VNIIGAZ, Moscow.